Vacuum Estimation of Error Field Correction on ASDEX Upgrade

D. Voltolina[1], P. Bettini[1,2], V. Igochine[3], L. Marrelli[2], R. McDermott[3], L. Pigatto[2], L. Piron[2], I. Zammuto[3], the ASDEX Upgrade Team[3], and the EUROfusion MST1 Team*

[1] *Centro Ricerche Fusione (CRF), University of Padova, 35127 Padova, Italy*

[2] *Consorzio RFX (CNR, ENEA, INFN, Università di Padova, Acciaierie Venete SpA), Corso Stati Uniti, 4 - Padova, Italy*

[3] *Max-Planck-Institut für Plasmaphysik, 85748 Garching, Germany*

Introduction

We present a study of the vacuum magnetic field produced by the Poloidal Field (PF) coil system of ASDEX Upgrade. Such a study aims at investigating possible sources of the error-fields (EFs) that have been already observed in AUG, as reported in [1, 2]. Moreover, EF correction (EFC) strategies, which should minimize the effect of EFs on plasma discharges by acting on the AUG *B-coil* system [3], are proposed. The results of this work have been applied to several discharges performed during the MST1-18-T09-AUG experimental campaign.

Numerical model of vacuum field

In order to model the vacuum field due to the PF coil system, either PF coils and their feedthroughs are considered. Assuming that the magnetic flux density field **B** due to PF coils is perfectly axisymmetric, it can be exactly reconstructed by the implementation of analytical formulas [4]. However, the symmetry of the poloidal field is distorted by the PF coils feedthroughs, so they are a source of EFs and their localized action may trigger locking modes as observed in [1]. From a modelling point of view, the contribute of feedthroughs to the total poloidal **B** field can be addressed by a 1-D model of such conductors. Indeed, the Biot-Savart law for the magnetic vector potential **A** and the magnetic flux density **B**, applied to a filamentary segment carrying a current I, gives the following expressions [5]:

$$\mathbf{A}(\mathbf{r}) = \frac{\mu_0 I}{4\pi} ln\left(\frac{R_i + R_f + L}{R_i + R_f - L}\right)\hat{\mathbf{e}} \tag{1}$$

$$\mathbf{B}(\mathbf{r}) = \frac{\mu_0 I}{4\pi}\frac{2L(R_i + R_f)}{R_i R_f}\frac{\hat{\mathbf{e}} \times \mathbf{R}_i}{(R_i + R_f)^2 - L^2} \tag{2}$$

where $\mathbf{r}$ is the observation point, $\mathbf{R}_i$ and $\mathbf{R}_f$ are the distance vectors between the starting and the ending point of the segment and $\mathbf{r}$ ($R_i = \|\mathbf{R}_i\|_2$, $R_f = \|\mathbf{R}_f\|_2$), L is the length of the filament and $\hat{\mathbf{e}}$ is the unit vector along the segment. If each feedthrough is modelled by a series of short segments, the non-axisymmetric contribute of the feedthroughs set to the total **A** and **B** results:

$$\mathbf{A}_{feed}(\mathbf{r}) = \sum_{h=1}^{N} \sum_{k=1}^{M_h} \mathbf{A}_{hk}(\mathbf{r}) \tag{3}$$

$$\mathbf{B}_{feed}(\mathbf{r}) = \sum_{h=1}^{N} \sum_{k=1}^{M_h} \mathbf{B}_{hk}(\mathbf{r}) \tag{4}$$

where N is the total number of feedthroughs, M_h is the number of segments of the h-th conductor, and $\mathbf{A}_{hk}$, $\mathbf{B}_{hk}$ are the contributes of its k-th segment, respectively.

Correction strategies

AUG is provided by a set of 16 in-vessel magnetic actuators (*B-coils*), which can be exploited for EFC purposes. Notably, in this work two EFC strategies derived by vacuum modelling are presented, which aim at minimizing the normal component of the non-axisymmetric field $\mathbf{B}_{feed}$ on rational q-surfaces, where EF components may trigger unstable modes and brake plasma rotation. Such EFC strategies have been identified by analysing a reference shot, originally without EFC, and tailoring the correction for the PF coil currents and the equilibrium quantities measured and computed for that shot. The vacuum computation of $\mathbf{B}$ field and the evaluation of the EFC currents are implemented in the CAFE-BS code, a version of CAFE code [6] used for the solution of electromagnetic stationary problems.

The first EFC strategy exploited relies on the minimization of the magnetic fluxes linked by a *Virtual Shell (VSh)*, made up of a set of virtual saddle loops that span a prescribed rational q-surface. Since these fluxes are proportional to the $\mathbf{B}_{feed}$ component normal to that surface, then the flux compensation should minimize the EFs due to feedthroughs as well. The virtual saddle loops are obtained projecting the traces of the 16 AUG *B-coils* on a desired flux surface (e.g. $q = 2$ or $q = 3$), as exemplified in Fig. 1. The flux ϕ_i linked by the i-th VSh loop, due to feedthroughs, can be computed discretizing the loop into a series of M_i filaments and recalling that $\mathbf{B} = \nabla \times \mathbf{A}$. It follows:

$$\phi_i = \int_{S_i} \mathbf{B}_{feed} \cdot \mathbf{n}\, ds = \int_{\partial S_i} \mathbf{A}_{feed} \cdot \mathbf{t}\, dl \approx \sum_{h=1}^{M_i} \int_{l_h} \mathbf{A}_{feed} \cdot \mathbf{t}_h\, dl \tag{5}$$

where S_i and ∂S_i are the surface of the loop and its boundary, while $\mathbf{t}$ and $\mathbf{t}_h$ are the unit vector tangent to ∂S_i and the unit vector along the h-th filament l_h in which ∂S_i is split. The last integral of (5) can be computed using (3) and applying a standard quadrature rule for line integrals. The fluxes linked by the 16 VSh loops are then stored into a vector of known terms $\boldsymbol{\phi}$. If a 1-D filamentary model is applied to the *B-coils* as well, (5) can be used to evaluate the mutual inductance between the i-th saddle loop and the j-th actuator, that is:

$$M_{ij} = \left. \frac{\phi_i}{I_j} \right|_{I_k=0} \quad \forall k \neq j \tag{6}$$

where I_j $(j = 1, ..., 16)$ is the current of the j-th *B-coil*. M_{ij} is stored as the (i, j) entry of the (16×16) matrix $\mathbf{M}$ of mutual inductances, such that the vector $\mathbf{I}$ of the *B-coils* correction

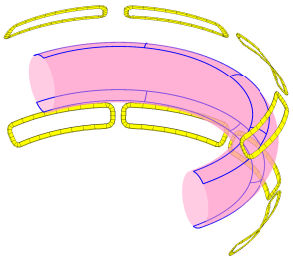

Figure 1: Virtual Shell (blue) as projection of B-coils (yellow) on a flux-surface (pink)

I_{uc}	I_{us}	I_{lc}	I_{ls}	(m,n) amplitude
1	0	0	0	C_{uc}
0	1	0	0	C_{us}
0	0	1	0	C_{lc}
0	0	0	1	C_{ls}

Table 1: Cosine and sine current components and relative harmonic amplitude

currents can be computed as $\mathbf{I} = \mathbf{M}^{-1}\boldsymbol{\phi}$. The second EFC strategy investigated is the Mode Control (MC) approach, which aims at minimizing a prescribed spatial harmonic pattern of the EFs on the desired q-surfaces. The amplitude E_{mn} of a prescribed (m,n) harmonic is obtained applying the Discrete Fourier Transform (DFT) to the normal component of $\mathbf{B}_{feed}$ computed on the prescribed $q = \frac{m}{n}$ surface. Assuming to minimize an $n = 1$ harmonic, the correction currents in the upper and lower set of B-coils should follow the same toroidal periodicity, thus:

$$I_{uj} = I_{uc}cos(\phi_{uj}) + I_{us}sin(\phi_{uj}) \quad , \quad I_{lj} = I_{lc}cos(\phi_{lj}) + I_{ls}sin(\phi_{lj}) \tag{7}$$

where I_{uj} (I_{lj}) is the current amplitude of the j-th coil of the upper (lower) set, located at the toroidal angle ϕ_{uj} (ϕ_{lj}), while I_{uc} (I_{lc}) and I_{us} (I_{ls}) are the cosine and sine component amplitudes respectively, independent from the toroidal angle, which defines the resulting current I_{uj} (I_{lj}) . One by one, each set of coils is supplied by a cosine or sine current pattern of unitary amplitude, then DFT yields the amplitudes C_{uc}, C_{us}, C_{lc}, C_{ls} of the selected (m,n) harmonic on the prescribed q-surface, as summarized in Tab. 1. The total (m,n) harmonic amplitude A_{mn} results:

$$A_{mn} = E_{mn} + C_{uc}I_{uc} + C_{us}I_{us} + C_{lc}I_{lc} + C_{ls}I_{ls} \tag{8}$$

An optimization algorithm can be used to rescale the four cosine and sine current components in order to minimize the object function A_{mn}.

Results and Comments

The EFC strategies described above have been calibrated using the reference shot #35352. The VSh approach aims at minimizing the total $\mathbf{B}_{feed}$ normal component on the computed $q = 2$ surface. MC is applied on the $q = 2$ and $q = 3$ surfaces in order to minimize the relative $(2,1)$ and $(3,1)$ EF harmonics together, by minimizing the total object function $A = \sqrt{A_{21}^2 + A_{31}^2}$. As shown in Fig. 2, being the EF pattern localized near the feedthroughs region, which spans almost $\pi/2$ (from $-\pi/4$ to $\pi/4$) of the toroidal machine extension, with a maximum value of approximately 0.25 mT, only the VSh loops close to that region are excited. This implies that a really localized action by means of few *B-coils* is required. Conversely, MC action may be considered as a global perturbation of the EF pattern, since an $n = 1$ distribution of currents is constrained, and a greater amplitude is required to compensate both the desired harmonics (Fig.

3). It is worth noting that VSh operates without any information on the harmonic spectra of EF: while MC is suppressing $(2,1)$ and $(3,1)$ components, VSh results in actually increasing them.

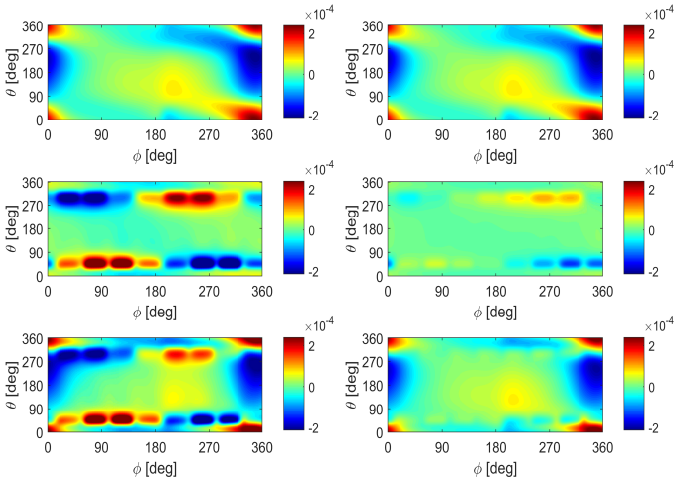

Figure 2: MC (left) and VSh (right) corrections on $q = 2$ surface (#35352). Top: total $\mathbf{B}_{feed}$, centre: correction field, bottom: resulting $\mathbf{B}$.

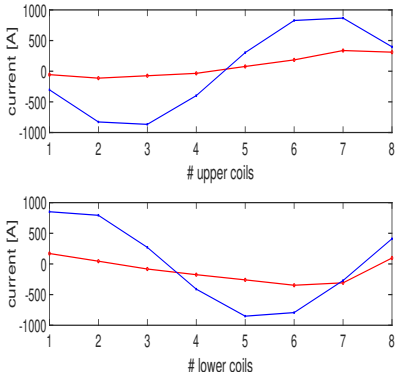

Figure 3: Correction currents of VSh (red) and MC (blue) computed for #35352.

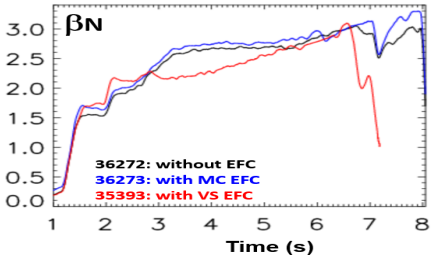

Figure 4: β_N (#36272, #36273, #35393). Black: no correction, blue: MC on $(2,1)$ and $(3,1)$, red: VSh.

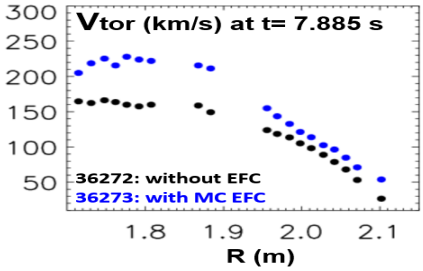

Figure 5: Plasma rotation (#36272, #36273). Black: no correction, blue: MC on $(2,1)$ and $(3,1)$ harmonics.

The EFC strategies above described have been tested when exploring high-β regimes in AUG. The VSh approach adopted for EFC (#35393) did not show any improvement in the plasma performance, compared to a similar shot without EFC (#35352). Conversely, the MC approach gave promising results. As shown in Fig. 4 and Fig. 5, in #36273 higher β_N and rotation values have been obtained compared with respect to a similar discharge without EFC (#36372). Further improvements of the model are foreseen, taking into account the effect of eddy-currents in the machine passive structures, as well as the plasma response by the use of MARS-F code [7].

[1] M. Maraschek, et al., Proc. 40th European Physical Society Conf. on Plasma Physics, P4.127 (Espoo, 2013)

[2] V. Igochine, et.al., 2017 Nucl. Fusion **57**, 116027

[3] W. Suttrop, et al., Fusion Engineering and Design **84**, 2 (2009)

[4] G. Chitarin, et al., IEEE Trans. Magn. **25**, 5 (1989)

[5] J.D. Hanson, and S.P. Hirshman, Physics of Plasmas **9**, 4410 (2002)

[6] P. Bettini, et al., Fusion Eng. Des. **123**, 528 (2017)

[7] Liu, Y.Q., et al., Physics of Plasmas **7**, 3681 (2000)

* See author list of B. Labit et.al. 2019 Nucl. Fusion accepted (https://doi.org/10.1088/1741-4326/ab2211)

This work has been carried out within the framework of the EUROfusion Consortium and has received funding from the Euratom research and training programme 2014-2018 and 2019-2020 under grant agreement No 633053. The views and opinions expressed herein do not necessarily reflect those of the European Commission.